Coulomb explosion of uniformly charged spheroids

M. Grech,[1,*] R. Nuter,[2] A. Mikaberidze,[1] P. Di Cintio,[1] L. Gremillet,[2] E. Lefebvre,[2] U. Saalmann,[1] J. M. Rost,[1] and S. Skupin[1,3]

[1]*Max-Planck-Institute for the Physics of Complex Systems, D-01187 Dresden, Germany*

[2]*CEA, DAM, DIF, F-91297 Arpajon, France*

[3]*Friedrich Schiller University, Institute of Condensed Matter Theory and Solid State Optics, D-07743 Jena, Germany*

(Received 1 May 2011; published 4 November 2011)

A simple, semianalytical model is proposed for nonrelativistic Coulomb explosion of a uniformly charged spheroid. This model allows us to derive the time-dependent particle energy distributions. Simple expressions are also given for the characteristic explosion time and maximum particle energies in the limits of extreme prolate and oblate spheroids as well as for the sphere. Results of particle simulations are found to be in remarkably good agreement with the model.

DOI: 10.1103/PhysRevE.84.056404 PACS number(s): 52.38.Kd, 52.38.Ph, 41.75.Jv, 52.27.Jt

I. INTRODUCTION

Coulomb explosion (CE) is an ubiquitous phenomenon in laser-matter interaction, from laser ablation and micromachining to particle acceleration [1–12]. CE is the dominant process of ion acceleration from a cluster irradiated by an intense laser pulse in the regime of so-called cluster vertical ionization (CVI) [1–6]. In this regime, the laser pulse is intense enough to remove all electrons from the cluster before ion motion sets in. This kind of ion charge state can also be generated by intense and short pulses of high-energy photons which have become possible at x-ray free electron lasers [13]. In both cases, the ion dynamics is governed by CE.

Spherical CE has been thoroughly investigated in the last years due to its importance for cluster physics. In the case of a uniformly charged sphere, CE is self-similar and can be described analytically [1–4]. The dynamics of CE of a nonuniformly charged sphere is more complex as it involves multiple flows so that a kinetic description is required [5,6].

In contrast, ellipsoidal and spheroidal (ellipsoidal with a rotational symmetry) CE has been studied in the context of accelerator physics, where three-dimensional (3D) envelope equations are widely used [14,15], or to model space charge effects in laser-created dense electron beams [16].

Spheroidal clusters have also attracted a lot of attention as they exhibit characteristic electron momentum distributions [17], and their optical properties are of great interest in, for example, nano-optics [18,19]. They may also be produced in the context of ultracold quasineutral plasma studies [20]. Moreover, spheroidal clusters appear as a natural candidate for anisotropic ion emission from clusters under intense ultrashort laser irradiation, which has recently triggered significant interest [21]. Finally, it has also been shown that, in helium embedded rare gas clusters, a spheroidal nanoplasma is generated by illumination with an intense laser pulse leading to unusual resonant heating [22].

In addition, understanding spheroidal CE is crucial in the context of ion acceleration from a solid target irradiated by an intense, relativistic laser pulse. Recent studies have shown CE of thin multispecies targets as a promising path toward high-quality ion beams [7–10]. Apart from the possibility to use CE as the principal acceleration mechanism, CE of the accelerated ion bunch itself has been shown to play a dominant role in angular as well as energy dispersion of ion beams generated from laser-solid interaction [10,11].

In this paper, we investigate the CE of an initially uniformly charged spheroid. In order to derive simple estimates for the particle maximum energies and characteristic explosion time, we restrict ourselves to nonrelativistic particle velocities. We then demonstrate that, during CE, both the spheroidal shape and uniformity of the charge distribution are conserved, but with time-dependent aspect ratio and charge density. Therefore, CE of a uniformly charged spheroid can be described using a simple, semianalytical model for the evolution of the spheroid radii. This model allows us to derive the temporal evolution of the particle energy distribution and maximum energies (along the spheroid principal axes) as a function of the spheroid initial aspect ratio, charge density, and total charge. Our theoretical predictions are then compared to 3D molecular dynamics (MD) and particle-in-cell (PIC) simulations. These simulation tools are the most widely used methods to model laser-cluster and laser-plasma interaction. However, they are known to be computationally costly, so that the results obtained in this paper are interesting for various applications, from nonspherical cluster CE to non-neutralized charged particle beam propagation through a vacuum.

The paper is structured as follows: Section II presents our semianalytical model. Predictions from the model are then compared to both MD simulations (Sec. III) and PIC simulations (Sec. IV). Finally, Sec. V summarizes our findings.

II. SEMIANALYTICAL MODEL FOR COULOMB EXPLOSION OF UNIFORMLY CHARGED SPHEROIDS

A. General considerations on uniformly charged spheroids

In this first section, we lay the basis for our simple model of CE of a uniformly charged spheroid. To do so, let us first recall the electrostatic potential at a position $\mathbf{x} = (x,y,z)$ inside a uniformly charged ellipsoid centered in $\mathbf{x} = 0$ and with radii w_x, w_y, and w_z along the directions x, y, and z,

*mickael.grech@gmail.com

TABLE I. Limits of the shape functions for the extreme prolate (cigar-shaped, $\alpha \ll 1$) and oblate (disk-shaped, $\alpha \gg 1$) spheroids, as well as for the sphere ($\alpha = 1$).

	$\alpha \ll 1$	$\alpha = 1$	$\alpha \gg 1$
$\zeta_0(\alpha)$	$\ln(2/\alpha)$	1	$\pi/(2\alpha)$
$\zeta_\parallel(\alpha)$	$\alpha^2[\ln(2/\alpha) - 1]$	1/3	1
$\zeta_\perp(\alpha)$	1/2	1/3	$\pi/(4\alpha)$

respectively [23]:

$$\phi(\mathbf{x}) = \pi k \rho_c w_x w_y w_z \times \int_0^\infty \left(1 - \frac{x^2}{w_x^2 + s} - \frac{y^2}{w_y^2 + s} - \frac{z^2}{w_z^2 + s}\right) \frac{ds}{\sqrt{\psi(s)}}, \quad (1)$$

where $k = (4\pi\epsilon_0)^{-1}$ and $\rho_c = Zen$ is the charge density (typically Z is the mean ion charge state and n is the ion density), and $\psi(s) = (w_x^2 + s)(w_y^2 + s)(w_z^2 + s)$.

Objects with a rotational symmetry are of particular importance for many applications such as cluster explosion or particle acceleration. Hence, we introduce the radial coordinate $r = \sqrt{y^2 + z^2}$ and restrict our study to the case of a spheroid: $w_x = w_\parallel$ and $w_y = w_z = w_\perp$ so that $\psi(s) = (w_\parallel^2 + s)(w_\perp^2 + s)^2$. Finally, one obtains for the electrostatic potential inside the spheroid:

$$\phi(x,r) = 2\pi k \rho_c [w_\perp^2 \zeta_0(\alpha) - \zeta_\parallel(\alpha) x^2 - \zeta_\perp(\alpha) r^2], \quad (2)$$

where we have introduced the spheroid aspect ratio $\alpha = w_\perp / w_\parallel$ and

$$\zeta_0(\alpha) = \frac{1}{2} \int_0^\infty \frac{ds}{(\alpha^2 + s)\sqrt{1 + s}}, \quad (3)$$

$$\zeta_\parallel(\alpha) = \frac{\alpha^2}{2} \int_0^\infty \frac{ds}{(\alpha^2 + s)(1 + s)^{3/2}}, \quad (4)$$

$$\zeta_\perp(\alpha) = \frac{\alpha^2}{2} \int_0^\infty \frac{ds}{(\alpha^2 + s)^2 \sqrt{1 + s}}. \quad (5)$$

In what follows, we refer to these functions as shape functions because they depend only on the spheroid aspect ratio. Equations (3)–(5) are here written in their compact, integral forms. These integrals can, however, be expressed as functions of inverse trigonometric and hyperbolic functions (see, e.g., Ref. [24]). The dependencies of these shape functions on α are given in Fig. 1. We also give their limits for the extreme prolate (cigar-shaped, $\alpha \ll 1$) and oblate (disk-shaped, $\alpha \gg 1$) spheroids, as well as for the sphere in Table I.

Equation (2) illustrates the well-known result that the electrostatic potential inside a uniformly charged spheroid is a quadratic function of the space coordinates. As for the electric field inside the uniformly charged spheroid, it can be easily expressed in cylindrical coordinates:

$$\mathbf{E}(x,r) = E_\parallel(x)\hat{\mathbf{x}} + E_\perp(r)\hat{\mathbf{r}}, \quad (6)$$

where $\hat{\mathbf{x}}$ and $\hat{\mathbf{r}}$ are the longitudinal and radial unit vectors, respectively, and

$$E_\parallel(x) = -\partial_x \phi(x,r) = 4\pi k \rho_c \zeta_\parallel(\alpha) x, \quad (7)$$

$$E_\perp(r) = -\partial_r \phi(x,r) = 4\pi k \rho_c \zeta_\perp(\alpha) r. \quad (8)$$

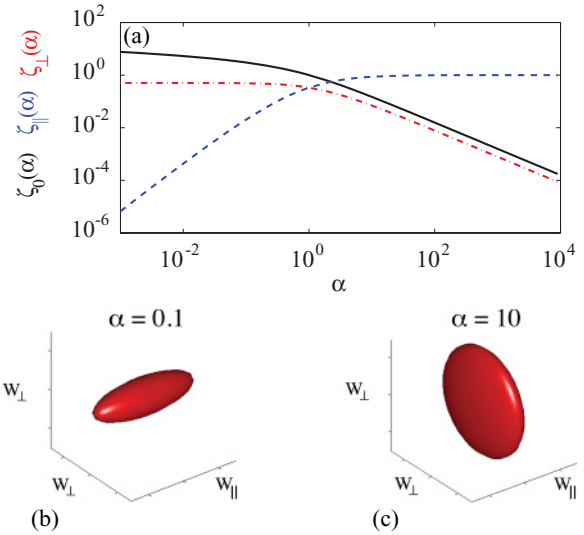

FIG. 1. (Color online) (a) Dependence of the shape functions $\zeta_0(\alpha)$ (solid black curve), $\zeta_\parallel(\alpha)$ (dashed blue curve), and $\zeta_\perp(\alpha)$ (dot-dashed red curve) on the aspect ratio α. (b) Prolate (cigar-shaped) spheroid with $\alpha = 0.1$ and (c) oblate (disk-shaped) spheroid with $\alpha = 10$.

Interestingly, besides the nontrivial dependency on the aspect ratio α, the longitudinal component of the electric field inside the spheroid is a linear function of x only, while the transverse component is a function of r only. The nonrelativistic equations of motion in such an electric field for a particle with charge Ze, mass m, and initial position (x_0, r_0) simply read

$$\frac{d^2}{dt^2}\tilde{x} = \kappa \zeta_\parallel(\alpha)\tilde{x}, \quad (9)$$

$$\frac{d^2}{dt^2}\tilde{r} = \kappa \zeta_\perp(\alpha)\tilde{r}, \quad (10)$$

where α and $\kappa = 4\pi k \rho_c (Ze/m)$ depend only on time, and $\tilde{x} = x/x_0$ and $\tilde{r} = r/r_0$. Considering initial conditions $\tilde{x}|_{t=0} = \tilde{r}|_{t=0} = 1$ and $\partial_t \tilde{x}|_{t=0} = \partial_t \tilde{r}|_{t=0} = 0$, Eqs. (9) and (10) are found to be independent of the initial coordinates x_0 and r_0. As a consequence, a particle initially located at a position (x_0, r_0) will subsequently be at a position $(x_0\tilde{x}, r_0\tilde{r})$, where $\tilde{x}$ and $\tilde{r}$ do not depend on the initial position. Therefore, it is straightforward to obtain that (i) the CE of an initially uniformly charged spheroid conserves the spheroidal shape (albeit, as we will see in Sec. II B, with a time-dependent aspect ratio), and that (ii) the charge distribution inside the spheroid remains uniform (albeit time dependent).

Although the above calculations have been performed considering Coulomb interaction in a spheroid, we would like to stress that similar conclusions can be drawn for the more general case of an ellipsoid, as well as for any Coulomb-like force, such as gravitation [25,26].

The above considerations strongly simplify the modeling of CE of a uniformly charged spheroid. The problem can now be solved by considering equations for the evolution of the longitudinal and transverse radii of the spheroid.

B. Coulomb explosion of uniformly charged spheroids

1. Governing equations

Let us consider a uniformly charged spheroid with initial radii $w_{\parallel,0}$ and $w_{\perp,0}$, and initial ion charge density n_0. Obviously, the total charge $Q = (4\pi/3)w_{\parallel,0}w_{\perp,0}^2(Zen_0)$ is conserved during the explosion. The nonrelativistic equations of motion (9) and (10) are also valid for particles initially located on the outer shell of the spheroid at $(x = w_{\parallel,0}, r = 0)$ and $(x = 0, r = w_{\perp,0})$. Then, using Eqs. (7) and (8), it is straightforward to derive a system of two second-order differential equations on the time-dependent longitudinal and transverse radii $w_\parallel$ and $w_\perp$:

$$\frac{d^2}{dt^2}w_\parallel = \omega_{p0}^2\frac{w_{\perp,0}^2 w_{\parallel,0}}{w_\perp^2}\zeta_\parallel\left(\frac{w_\perp}{w_\parallel}\right), \tag{11}$$

$$\frac{d^2}{dt^2}w_\perp = \omega_{p0}^2\frac{w_{\perp,0}^2 w_{\parallel,0}}{w_\perp w_\parallel}\zeta_\perp\left(\frac{w_\perp}{w_\parallel}\right), \tag{12}$$

where we have introduced the plasma frequency

$$\omega_{p0} = \sqrt{Z^2e^2n_0/(\epsilon_0 m)}. \tag{13}$$

Let us now normalize the time to ω_{p0}^{-1} ($\tau = \omega_{p0}t$), the longitudinal radius to $w_{\parallel,0}$ ($\tilde{w}_\parallel = w_\parallel/w_{\parallel,0}$), and the transverse radius to $w_{\perp,0}$ ($\tilde{w}_\perp = w_\perp/w_{\perp,0}$). The system of Eqs. (11) and (12) then reads

$$\frac{d^2}{d\tau^2}\tilde{w}_\parallel = \frac{1}{\tilde{w}_\perp^2}\zeta_\parallel\left(\alpha_0\frac{\tilde{w}_\perp}{\tilde{w}_\parallel}\right), \tag{14}$$

$$\frac{d^2}{d\tau^2}\tilde{w}_\perp = \frac{1}{\tilde{w}_\perp\tilde{w}_\parallel}\zeta_\perp\left(\alpha_0\frac{\tilde{w}_\perp}{\tilde{w}_\parallel}\right), \tag{15}$$

where $\alpha_0 = w_{\perp,0}/w_{\parallel,0}$ is the spheroid initial aspect ratio. Assuming that all particles in the spheroid have initially no velocity, one has for initial conditions

$$\tilde{w}_\parallel(\tau = 0) = 1, \quad \tilde{w}_\perp(\tau = 0) = 1, \tag{16}$$

$$\frac{d}{d\tau}\tilde{w}_\parallel(\tau = 0) = 0, \quad \frac{d}{d\tau}\tilde{w}_\perp(\tau = 0) = 0. \tag{17}$$

Note that Eq. (17) also implies that particles have no initial temperature. For bare ion spheroids, this situation arises when electron removal is fast enough for ion heating through electron-ion collisions to be negligible. Under such circumstances, the hypothesis of uniform charge density should also be verified as long as the initial atomic density is uniform.

Before discussing in more details the solution of this system, we note that, using these normalizations, velocities in the longitudinal and transverse directions are naturally expressed in units of $\omega_{p0}w_{\parallel,0}$ and $\omega_{p0}w_{\perp,0}$, respectively. Correspondingly, energies in the longitudinal and transverse directions are normalized to $\mathcal{E}_{\parallel,0} = \mathcal{E}_0/\alpha_0$ and $\mathcal{E}_{\perp,0} = \alpha_0\mathcal{E}_0$, respectively, where we have introduced the characteristic energy

$$\mathcal{E}_0 = \sqrt{\mathcal{E}_{\parallel,0}\mathcal{E}_{\perp,0}} = m\omega_{p0}^2 w_\parallel w_\perp. \tag{18}$$

Due to the complex dependency of the shape functions on the time-dependent aspect ratio, no general (for any α_0) analytical solution can be obtained and the system of Eqs. (14) and (15) has to be solved numerically. However, analytical solutions of the system can be obtained in the case of the sphere (where the aspect ratio remains constant in time $\tilde{w}_\perp/\tilde{w}_\parallel = \alpha_0 = 1$), in the case of an infinitely large disk ($\alpha_0 \to +\infty$ and considering $\alpha_0\tilde{w}_\perp/\tilde{w}_\parallel \to +\infty$ for all times), and in the case of an infinitely long cylinder ($\alpha_0 \to 0$ and considering $\alpha_0\tilde{w}_\perp/\tilde{w}_\parallel \to 0$ for all times). We present briefly the analytical solutions for these particular cases (Sec. II B 2) before discussing in more details the numerical solutions for arbitrary initial values of α_0 (Sec. II B 3).

2. Particular cases

a. Coulomb explosion of a uniformly charged sphere. Spherical CE ($\alpha_0 = 1$) has been widely studied in the context of many applications (e.g., in cluster physics [1–6]). In this case, the system of Eqs. (14) and (15) reduces to a single differential equation on the sphere radius $\tilde{R} = \tilde{w}_\parallel = \tilde{w}_\perp$:

$$\frac{d^2}{d\tau^2}\tilde{R} = \frac{1}{3\tilde{R}^2}. \tag{19}$$

The first integral of Eq. (19) is obtained after multiplying both sides by $\frac{d}{d\tau}\tilde{R}$ and integrating from 0 to τ. Considering that all particles have initially no velocity, we obtain

$$\frac{1}{2}\left(\frac{d}{d\tau}\tilde{R}\right)^2 = \frac{1}{3}\left(1 - \frac{1}{\tilde{R}}\right). \tag{20}$$

This equation describes the transformation of potential energy [right-hand side (rhs) of Eq. (20)] to kinetic energy [left-hand side (lhs) of Eq. (20)] for a particle located on the outer shell of the spheroid. In our normalized units, energies $\tilde{\mathcal{E}}$ are expressed in units of $\mathcal{E}_{\parallel,0} = \mathcal{E}_{\perp,0} = \mathcal{E}_0 = m\omega_{p0}^2R_0^2$, where R_0 is the initial radius of the sphere and ω_{p0} is given by Eq. (13). The final kinetic energy of an ion of the sphere outer shell is therefore

$$\mathcal{E}_S = \mathcal{E}_0/3. \tag{21}$$

The autonomous differential equation (20) has a formal implicit solution

$$\tau = \sqrt{\frac{3}{2}}\int_1^{\tilde{R}}\sqrt{\frac{r}{r-1}}\,dr. \tag{22}$$

This solution and the temporal evolution of the outer shell kinetic energy $\mathcal{E}_{\max}$ are shown in Fig. 2. On long time scales ($\tau = \omega_{p0}t \gg 1$), we find $\tilde{R} \sim \sqrt{2/3}\tau$; that is, most of the potential energy has been transformed into kinetic energy and the sphere expands with the constant velocity $\sqrt{2/3}\omega_{p0}R_0$. On shorter time scales we actually observe the Coulomb explosion; that is, 50% of the potential energy is transformed into kinetic energy after a time $\tau \simeq 2.8$, while 80% is transformed after $\tau \simeq 7.2$. The characteristic time scale of spherical explosion is therefore the inverse initial plasma frequency ω_{p0}^{-1}.

Following Refs. [1,2,4], we can derive an analytical expression for the asymptotic ($t \to \infty$) particle energy distribution. As previously underlined, in our model, the electric field inside the sphere is a linear function of the radius and particles do not overtake each other during expansion. The electric field seen by a particle initially located at $\tilde{r}_0 \leqslant 1$ can thus be easily obtained as a function of the charge $q(\tilde{r}_0)$ inside the sphere

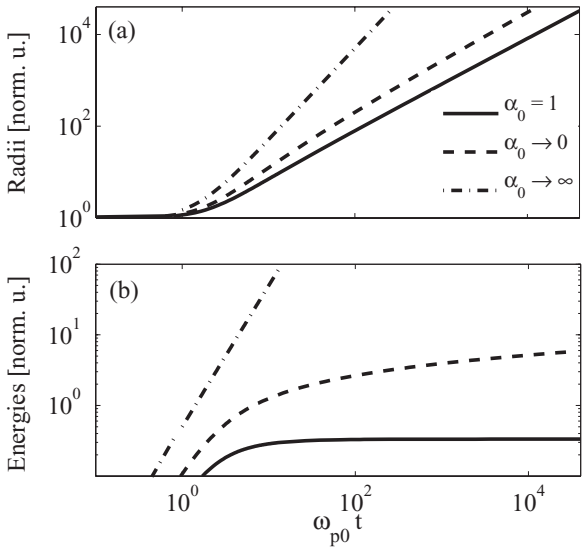

FIG. 2. Temporal evolution of (a) normalized spheroid radii (R/R_0, $w_\parallel/w_{\parallel,0}$, and $w_\perp/w_{\perp,0}$), and (b) maximum kinetic energies ($\mathcal{E}_{\max}/\mathcal{E}_0$, $\mathcal{E}_{\parallel,\max}/\mathcal{E}_{\parallel,0}$, and $\mathcal{E}_{\perp,\max}/\mathcal{E}_{\perp,0}$) for spherical explosion (solid curves), cylindrical explosion (dashed curves), and planar explosion (dot-dashed curves), respectively.

with normalized radius $\tilde{r}_0$. The equation of motion for this particle then reads

$$\frac{d^2}{d\tau^2}\tilde{r} = \frac{\tilde{r}_0^3}{3\tilde{r}^2}. \tag{23}$$

Then the first integral simply reads (assuming zero initial velocity)

$$\frac{1}{2}\left(\frac{d}{d\tau}\tilde{r}\right)^2 = \frac{\tilde{r}_0^3}{3}\left(\frac{1}{\tilde{r}_0} - \frac{1}{\tilde{r}}\right). \tag{24}$$

This equation once more describes energy conservation and shows that an ion initially located at a position $\tilde{r}_0$ has obtained, at the end of the acceleration process, a kinetic energy $\tilde{\mathcal{E}}(\tilde{r}_0) = \tilde{r}_0^2/3$. Now, the normalized radial particle density at initial position $\tilde{r}_0$ is simply

$$\frac{dN}{d\tilde{r}_0} = 3\tilde{r}_0^2\theta_H(1-\tilde{r}_0), \tag{25}$$

where θ_H is the Heaviside function, from which we derive the ion energy distribution at $t \to \infty$:

$$\frac{dN}{d\tilde{\mathcal{E}}} = \frac{dN}{d\tilde{r}_0}\frac{d\tilde{r}_0}{d\tilde{\mathcal{E}}} = \frac{9}{2}\sqrt{3\tilde{\mathcal{E}}}\theta_H(1/3-\tilde{\mathcal{E}}). \tag{26}$$

Hence, one obtains that the particle energy distribution scales as the square-root of the ion energy up to the maximum energy $\tilde{\mathcal{E}}^\infty = 1/3$.

At this point, we want to stress that this asymptotic energy distribution can actually be generalized to all times t. It is indeed well known that CE of a uniformly charged sphere is self-similar and that the velocity distribution inside the sphere increases linearly with distance to its center. From this we can derive the fraction of particles with energy below $\mathcal{E} \leqslant \mathcal{E}_{\max}(t)$: $N(\mathcal{E}) = [\mathcal{E}/\mathcal{E}_{\max}(t)]^{3/2}$, where $\mathcal{E}_{\max}(t)$ is the maximum particle energy at time t. We finally obtain the time-dependent spectrum:

$$\frac{dN}{d\mathcal{E}} = \frac{3}{2}\frac{\sqrt{\mathcal{E}}}{\mathcal{E}_{\max}^{3/2}(t)}\theta_H[\mathcal{E}_{\max}(t)-\mathcal{E}]. \tag{27}$$

b. Coulomb explosion of a uniformly charged, infinitely long cylinder. In the case of a uniformly charged, infinitely long cylinder, the system of Eqs. (14) and (15) reduces to a single differential equation for the cylinder radius $\tilde{w}_\perp$:

$$\frac{d^2}{d\tau^2}\tilde{w}_\perp = \frac{1}{2\tilde{w}_\perp}. \tag{28}$$

Once more, the first integral of Eq. (28) describes energy conservation:

$$\frac{1}{2}\left(\frac{d}{d\tau}\tilde{w}_\perp\right)^2 = \frac{1}{2}\ln\tilde{w}_\perp. \tag{29}$$

In contrast to the spherical case considered above, the logarithmic potential on the rhs of Eq. (29) goes to infinity for increasing $\tilde{w}_\perp$. This unphysical behavior follows from our choice of an infinitely long (thus with infinite total charge) cylinder. As a result, the energy of the outer shell formally diverges.

Again a formal implicit solution can be obtained for the cylinder radius:

$$\tau = \int_1^{\tilde{w}_\perp}\frac{dw}{\sqrt{\ln w}}. \tag{30}$$

The temporal evolution of $\tilde{w}_\perp$ and the outer shell energy $\mathcal{E}_\perp$ are presented in Fig. 2. Expansion occurs with an increasing velocity, and no saturation of the kinetic energy is observed.

c. Coulomb explosion of a uniformly charged, infinitely large disk. In the case of a uniformly charged, infinitely large disk, the system of Eqs. (14) and (15) reduces to a single differential equation for the disk thickness $\tilde{w}_\parallel$:

$$\frac{d^2}{d\tau^2}\tilde{w}_\parallel = 1. \tag{31}$$

In this case, the disk thickness increases due to a constant electrostatic field. It simply reads

$$\tilde{w}_\parallel = \frac{\tau^2}{2} + 1. \tag{32}$$

This result is shown in Fig. 2. In this case as well, no stationary state is obtained and the kinetic energy increases arbitrarily.

3. Numerical solutions for an arbitrary initial aspect ratio

As previously discussed, in the general case (for any initial aspect ratio α_0), the system of Eqs. (14) and (15) must be solved numerically. In this paper, it is done using a simple Euler method. Numerical solutions for different values of α_0 are now discussed.

Figure 3 shows the temporal evolution of the longitudinal and transverse radii of the spheroid [Figs. 3(a) and 3(b), respectively] and of the longitudinal and transverse kinetic energies [Figs. 3(c) and 3(d), respectively]. It is complemented by Fig. 4 which shows, as a function of the initial aspect ratio α_0, the times required for the kinetic energy (for purely longitudinal or purely transverse motion) to reach 50% or 80%

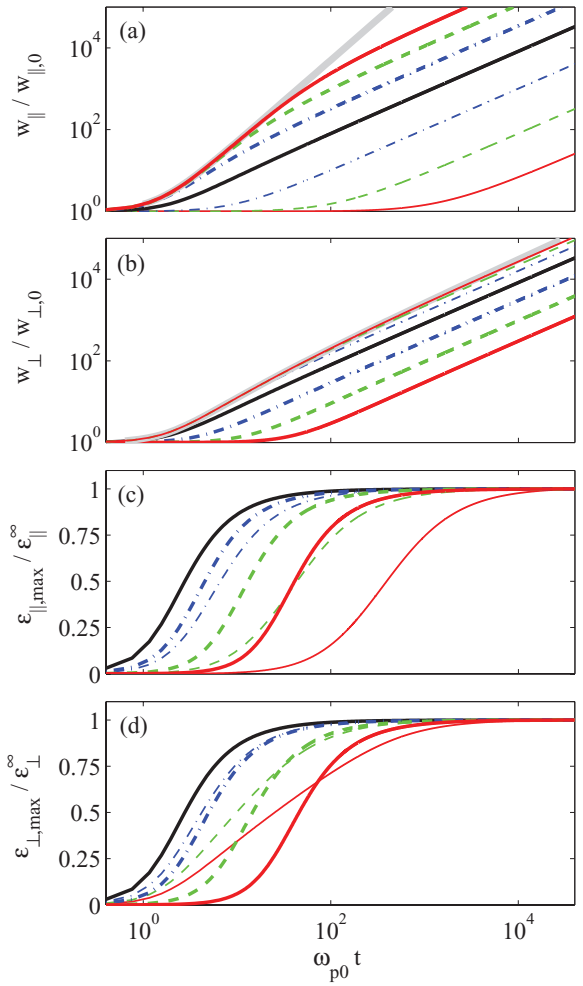

FIG. 3. (Color online) Temporal evolution of spheroidal Coulomb explosion for different values of the initial aspect ratio α_0: (a) longitudinal radius of the spheroid, (b) transverse radius of the spheroid, (c) energy associated with longitudinal motion, and (d) energy associated with transverse motion. Color codes are as follows: Prolate spheroid (thin curves, $\alpha_0 = 10^{-3}$ solid red, $\alpha_0 = 10^{-2}$ dashed green, and $\alpha_0 = 10^{-1}$ dot-dashed blue). Sphere (solid black curve, $\alpha_0 = 1$). Oblate spheroid (thick curves, $\alpha_0 = 10^3$ solid red, $\alpha_0 = 10^2$ dashed green, and $\alpha_0 = 10$ dot-dashed blue). The thick solid gray curves in panels (a) and (b) show analytical predictions for planar ($\alpha_0 \to \infty$) and cylindrical ($\alpha_0 \to 0$) explosion, respectively. Note that energies in panels (c) and (d) are normalized to their asymptotic values at $t \to \infty$.

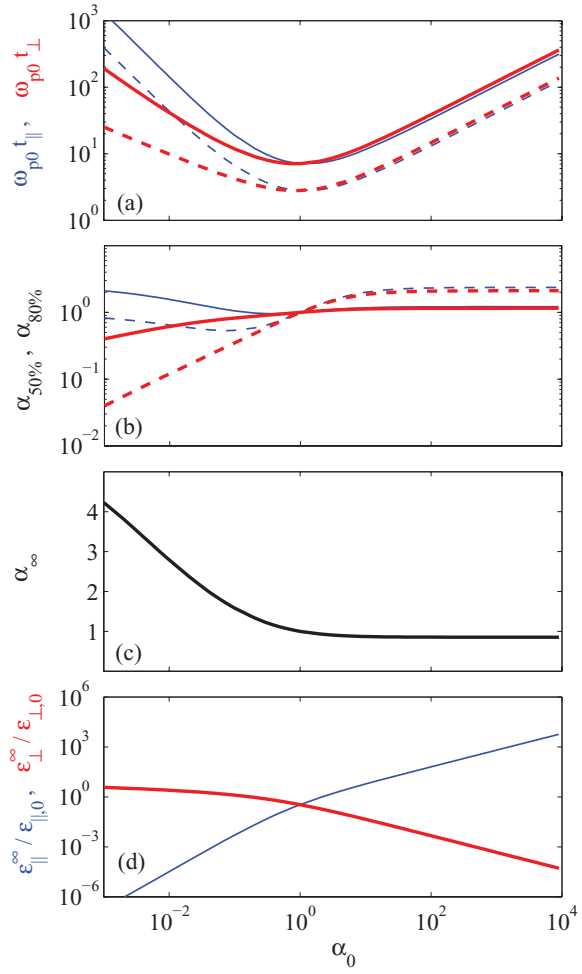

FIG. 4. (Color online) Dependence on initial aspect ratio α_0 of (a) time to reach 50% (dashed curves) or 80% (solid curves) of maximum kinetic energy, (b) corresponding intermediate aspect ratio $\alpha_0\tilde{w}_\perp/\tilde{w}_\parallel$, (c) final aspect ratio α_∞, and (d) final energies $\mathcal{E}_\parallel^\infty$ and $\mathcal{E}_\perp^\infty$ normalized to $\mathcal{E}_{\parallel,0}$ and $\mathcal{E}_{\perp,0}$, respectively. In panels (a), (b), and (d), thin blue curves account for motion in the longitudinal direction, and thick red curves account for motion in the transverse direction.

of its maximum value [Fig. 4(a)], the corresponding aspect ratio of the spheroid at these times [Fig. 4(b)], the final aspect ratio α_∞ [Fig. 4(c)], and the final energies normalized to $\mathcal{E}_{\parallel,0}$ and $\mathcal{E}_{\perp,0}$ [Fig. 4(d)].

Let us first address the case of spherical explosion ($\alpha_0 = 1$). Numerical solutions allow us to recover the analytical findings of Sec. II B 2. The radius and energy evolutions (Fig. 3) are in perfect agreement with what is presented in Fig. 2. It is also worth pointing out that, for a given initial charge density (i.e., for a fixed value of ω_{p0}), spherical expansion is faster (in terms of energy conversion) than for any other initial aspect ratio α_0. This can be observed in Figs. 3(c) and 3(d), as well as in Fig. 4(a), where the characteristic time to reach a given fraction of the final kinetic energy reaches a minimum for $\alpha_0 = 1$. Finally, we recall that the characteristic time for spherical CE is of the order of ω_{p0}^{-1} and the final velocities of the outer shell in the longitudinal and transverse directions are $v_{\parallel,\max}(t \to \infty) = v_{\perp,\max}(t \to \infty) = \sqrt{2/3}\omega_{p0}R_0$.

In the case of a prolate (cigar-shaped, $\alpha_0 \ll 1$) spheroid, expansion occurs mainly in the transverse plane. This intuitive result is illustrated in Figs. 3(a) and 3(b) where the transverse radius of the spheroid increases much faster than the longitudinal one. Note that, although the transverse radius of the prolate spheroid evolves initially faster than in the spherical case, spherical expansion remains faster in terms of conversion from potential to kinetic energy [Fig. 4(d)]. The quasistationary state of expansion (i.e., expansion at quasiconstant velocity) is indeed reached later for $\alpha_0 \neq 1$. Note also that saturation in the kinetic energy arises once the spheroid assumes a quasispherical shape: when the kinetic energy reaches 80% of its maximum value, the spheroid aspect ratio is indeed quite close to unity [Fig. 4(b)]. The final aspect ratio is nevertheless

much larger than unity as the final transverse velocity is much larger than the longitudinal one. We also see from Fig. 4(a) that spheroidal expansion in the limit $\alpha_0 \ll 1$ occurs on a time scale larger than $(\alpha_0\omega_{p0})^{-1}$. Similarly, we see in Fig. 4(d) that the asymptotic ($t \to \infty$) energy for purely longitudinal motion $\mathcal{E}_\parallel^\infty$ does not exceed $\alpha_0^2\mathcal{E}_{\parallel,0} = \alpha_0\mathcal{E}_0$ while the corresponding energy for purely transverse motion $\mathcal{E}_\perp^\infty > \mathcal{E}_0/3$ (for example, for $10^{-5} < \alpha_0 < 10^{-1}$, we find that $\mathcal{E}_\perp^\infty$ ranges between $\mathcal{E}_{\perp,0} = \alpha_0\mathcal{E}_0$ and $7\mathcal{E}_{\perp,0} = 7\alpha_0\mathcal{E}_0$). The final transverse energy is therefore significantly larger than the longitudinal energy (see also theoretical predictions in Fig. 6). This is a consequence of the initial geometry, and it is responsible for the final oblate shape of the spheroid observed in Fig. 4(b).

Let us now focus on the case of an oblate (disk-shaped, $\alpha_0 \gg 1$) spheroid which is particularly interesting when considering laser-generated ion bunches from a solid target. As expected, expansion initially occurs in the longitudinal direction [Figs. 3(a) and 3(b)]. Transverse expansion eventually occurs later, once the spheroid longitudinal radius becomes comparable to its transverse one. At this time, the spheroid aspect ratio becomes close to unity and a non-negligible fraction of the potential energy has already been converted into kinetic energy [Fig. 4(b)]. Finally, one can extract from the numerical results the characteristic expansion time in the limit of large initial aspect ratio to be $\propto \sqrt{\alpha_0}/\omega_{p0}$. The asymptotic maximum energies can also be easily extracted: $\mathcal{E}_\parallel^\infty \sim 0.63\alpha_0\mathcal{E}_{\parallel,0} = 0.63\mathcal{E}_0$ and $\mathcal{E}_\perp^\infty \sim 0.46\mathcal{E}_{\perp,0}/\alpha_0 = 0.46\mathcal{E}_0$. We thus obtain that the final energies in the longitudinal and transverse directions are of the same order. This leads to a final aspect ratio $\alpha_\infty \sim (\mathcal{E}_\perp^\infty/\mathcal{E}_\parallel^\infty)^{1/2} \simeq 0.86$, close to unity, as shown in Fig. 4(c).

C. Energy spectra

Our model for spheroidal CE allows us to derive the maximum energies for motion along the spheroid principal axes at time t. As the density inside the spheroid remains uniform, the velocity distribution along the principal axes has to be a linear function of spatial coordinates:

$$v_\parallel(x) = (x/w_\parallel)v_{\parallel,\max}, \tag{33}$$

$$v_\perp(r) = (r/w_\perp)v_{\perp,\max}, \tag{34}$$

where $w_\parallel$, $w_\perp$ are the spheroid radii, and $v_{\parallel,\max}$ and $v_{\perp,\max}$ are the particle maximum velocities at a given time t. Considering a homogeneous charge density in the spheroid, one can easily derive the time-dependent normalized energy distribution for motion along the longitudinal and transverse directions [cf. Eq. (27)]:

$$\frac{dN}{d\mathcal{E}_\parallel} = \frac{3}{2}\frac{\sqrt{\mathcal{E}_\parallel}}{\mathcal{E}_{\parallel,\max}^{3/2}}\theta_H(\mathcal{E}_{\parallel,\max} - \mathcal{E}_\parallel), \tag{35}$$

$$\frac{dN}{d\mathcal{E}_\perp} = \frac{3}{2}\frac{\sqrt{\mathcal{E}_\perp}}{\mathcal{E}_{\perp,\max}^{3/2}}\theta_H(\mathcal{E}_{\perp,\max} - \mathcal{E}_\perp), \tag{36}$$

where $\mathcal{E}_{\parallel,\max} = mv_{\parallel,\max}^2/2$ and $\mathcal{E}_{\perp,\max} = mv_{\perp,\max}^2/2$ are time dependent and derived from our model.

The total energy spectrum can also be derived by considering equivelocity surfaces as concentric homeoids (spheroidal surfaces). We obtain from Eqs. (33) and (34) that these homeoids are actually similar; that is, they have the same aspect ratio $\alpha_v = (w_\perp/w_\parallel)v_{\parallel,\max}/v_{\perp,\max}$ at fixed time t (see Fig. 5) [27]. This allows us to calculate, for a given energy $\mathcal{E}$, the fraction $N(\mathcal{E})$ of particles in the spheroid with a lower energy and finally derive the normalized energy distribution.

For a prolate (cigar-shaped, $\alpha_0 < 1$) spheroid, the total energy spectrum reads

$$\frac{dN}{d\mathcal{E}} = \frac{3}{2}\begin{cases}\dfrac{\sqrt{\mathcal{E}/\mathcal{E}_{\parallel,\max}}}{\mathcal{E}_{\perp,\max}} & \text{for } \mathcal{E} < \mathcal{E}_{\parallel,\max} \\ \dfrac{1}{\mathcal{E}_{\perp,\max}}\sqrt{\dfrac{\mathcal{E}_{\perp,\max}-\mathcal{E}}{\mathcal{E}_{\perp,\max}-\mathcal{E}_{\parallel,\max}}} & \text{for } \mathcal{E}_{\parallel,\max} < \mathcal{E} < \mathcal{E}_{\perp,\max}.\end{cases} \tag{37}$$

For an oblate (disk-shaped, $\alpha_0 > 1$) spheroid, the total energy spectrum reads

$$\frac{dN}{d\mathcal{E}} = \frac{3}{2}\begin{cases}\dfrac{\sqrt{\mathcal{E}/\mathcal{E}_{\parallel,\max}}}{\mathcal{E}_{\perp,\max}} & \text{for } \mathcal{E} < \mathcal{E}_{\perp,\max} \\ \dfrac{\sqrt{\mathcal{E}/\mathcal{E}_{\parallel,\max}}}{\mathcal{E}_{\perp,\max}} - \dfrac{1}{\mathcal{E}_{\perp,\max}}\sqrt{\dfrac{\mathcal{E}-\mathcal{E}_{\perp,\max}}{\mathcal{E}_{\parallel,\max}-\mathcal{E}_{\perp,\max}}} & \text{for } \mathcal{E}_{\perp,\max} < \mathcal{E} < \mathcal{E}_{\parallel,\max}.\end{cases} \tag{38}$$

In the next sections (Secs. III and IV), we compare these predictions from our model to MD and PIC simulations.

III. MOLECULAR DYNAMICS SIMULATIONS

Molecular dynamics [28] simulations of CE of an (initially) uniformly charged spheroid are now discussed. To initialize our simulations, $N = 5000$ particles (here, hydrogen ions; $Z = 1$, $m = 1836m_e$, where m_e is the electron mass) are randomly placed within a spheroidal volume so that the initial particle density inside this volume is homogeneous. Here we chose an atomic density $n_0 \simeq 9.7 \times 10^{22}$ cm^{-3} (correspondingly, the sphere radius is $R_0 \simeq 2.3$ nm), which is characteristic of hydrogen clusters. To avoid unphysically large contributions to the energy spectrum, we enforce a minimum interparticle distance ($\simeq$75% of the average interparticle distance $d_{\min} \sim n_0^{-1/3}$). Furthermore, all particles were taken initially at rest. Then, knowing the initial state of all particles, we solve Newton's (nonrelativistic) equations of motion for each of them using the velocity Verlet scheme [29,30] and direct calculation of the Coulomb forces between all ions.

Several simulations were performed only changing the initial aspect ratio in the range $\alpha_0 = 0.1$ to 10. Figure 6 shows the maximum energy for longitudinal and transverse motion as predicted by our semianalytical model (Sec. II) and as

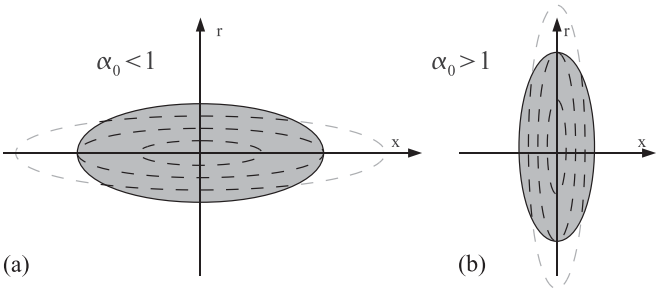

FIG. 5. Schematic representation of equivelocity surfaces at fixed time t during CE of (a) prolate (cigar-shaped, $\alpha_0 < 1$) spheroid and (b) oblate (disk-shaped, $\alpha_0 > 1$) spheroid. In this two-dimensional representation, equivelocity surfaces correspond to concentric ellipses with the same aspect ratio.

extracted from MD simulations. We stress that, here, energies are normalized to the maximum energy $\mathcal{E}_S$ [Eq. (21)] resulting from CE of a sphere with similar density and total charge (in practical units, $\mathcal{E}_S \simeq 3.1$ keV under current conditions). Figure 6 shows a rather good agreement between our simplified model [solutions of Eqs. (14) and (15)] and simulations. Also note that MD results confirm the theoretical prediction (clearly shown in Fig. 6) that, for a given total charge and charge density in the spheroid, the maximum longitudinal (transverse) energy is obtained for a slightly oblate (prolate) spheroid.

To further investigate MD simulation results, we present in Fig. 7 the energy spectra obtained at the end of the simulation [at a time $t \simeq 400\omega_{p0}^{-1}$ (and $\omega_{p0}^{-1} \simeq 2.4$ fs)] and compare them to theoretical predictions from Eqs. (27) and (35)–(38). Distributions in longitudinal (transverse) energy are obtained by considering particles emitted within an angle $\theta = \pm\pi/20$ around the longitudinal (transverse) direction. Figures 7(a) and 7(b) correspond to spherical CE ($\alpha_0 = 1$). In this case, the energy distribution is in very good agreement with the

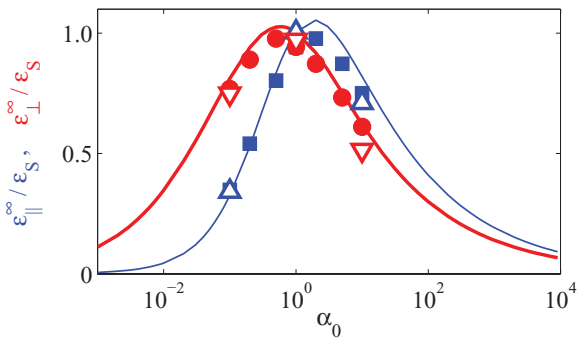

FIG. 6. (Color online) Dependence of the maximum energy for the longitudinal and transverse motions (thin blue and thick red curves, respectively) on the initial aspect ratio α_0. Solid lines correspond to semianalytical predictions [Eqs. (14) and (15)], circles and squares correspond to the maximum transverse and longitudinal energies obtained in MD simulation results, and triangles correspond to PIC simulation results (up-triangles and down-triangles correspond to longitudinal and transverse energies, respectively). Note that energies are normalized to the asymptotic energy $\mathcal{E}_S = \mathcal{E}_0/3$ [Eq. (21)] obtained for spherical explosion.

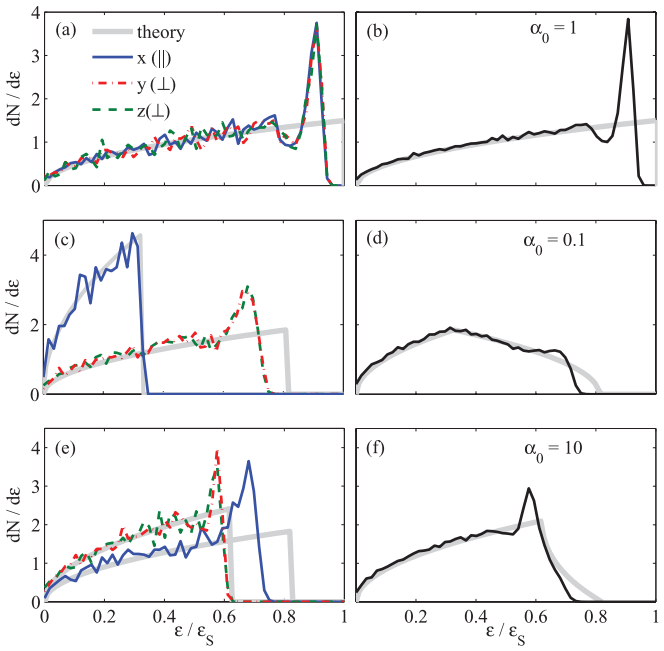

FIG. 7. (Color online) Energy spectra obtained from MD simulations at $t \simeq 400\omega_{p0}^{-1}$: Panels (a) and (b) are for $\alpha_0 = 1$, panels (c) and (d) are for $\alpha_0 = 0.1$, and panels (e) and (f) are for $\alpha_0 = 10$. The left panels (a), (c), and (e) show the directional spectra: the solid blue curves correspond to particles emitted within an angle $\pm\pi/20$ of the longitudinal (x) direction, the dashed green curves and dot-dashed red curves correspond to particles emitted within an angle $\pm\pi/20$ of the transverse (z and y) directions. The right panels (b), (d), and (f) show the total energy spectra (all particles are accounted for). The thick gray lines show the theoretical predictions from our model.

theoretical prediction from Eq. (27) for energies up to 90% of the maximum energy. Near the maximum energy, however, a peak appears in the simulation which is not predicted by our model.

Figures 7(c), 7(d), and 7(e), 7(f) show similar results for CE of a prolate (cigar-shaped, $\alpha_0 = 0.1$) spheroid and an oblate (disk-shaped, $\alpha_0 = 10$) spheroid, respectively. Once more, a very good agreement is obtained between theoretical predictions from our model and MD simulations. Only at the maximum energy is a peak observed for any direction of emission in the MD spectra, which is absent in the model spectra.

All the peaks observed at high energies are a consequence of the discrete nature of particles, which leads to a gradual decrease in the particle density at the surface of the spheroid. The thickness of the corresponding surface layer is of the order of the average interparticle separation. The decreasing density results in ion wave breaking (or formation of a shock), whose characteristic signature is a peak in the energy spectrum [5,6,31,32]. The peak is found to be sensitive to the initial particle distribution and its magnitude decreases with the increase of the total number of particles. This behavior is captured by the MD calculations, which take into account the motion of discrete ions, but is neglected in our simplified model, which considers the evolution of a continuous particle density with a sharp cutoff at the surface.

IV. PARTICLE-IN-CELL SIMULATIONS

We now present results from simulations of spheroidal CE obtained using the massively parallel 3D PIC code CALDER [33]. The PIC simulation technique consists of solving the Maxwell-Vlasov system and thus offers a mean-field kinetic description for the plasma dynamics [34]. In PIC codes, the Vlasov equation is solved by discretizing the particle distribution functions as a sum of so-called macroparticles and by solving, for each of these macroparticles, the corresponding (relativistic) equation of motion in the electromagnetic field. Then, the Maxwell-Ampère and Maxwell-Faraday equations are solved on a Yee mesh using the finite-difference time-domain method [35]. This numerical scheme, coupled to the standard current and charge deposition algorithm in a PIC code, does not automatically satisfy the Poisson equation, which has to be enforced by correcting the electric fields at each time step. In CALDER, this is done by using the usual technique proposed by Boris [36]. We stress this point because this study presents simulations of an initially strongly non-neutral plasma for which it is of the utmost importance to accurately correct the electric field at all time steps. This difficulty can, however, be alleviated by using charge-conserving algorithms such as the one proposed by Esirkepov [37]. In this case indeed, the Poisson equation has to be solved only at the first time-step.

Now we present simulation results of spheroidal CE for three different values of the initial aspect ratio: $\alpha_0 = 0.1, \alpha_0 = 1$, and $\alpha_0 = 10$. All three spheroids consist of fully ionized carbon ions ($Z = 6$, $m = 12 \times 1836 m_e$) with density $n_0 \simeq 9.2 \times 10^{21}$ cm^{-3} and total charge $Q \simeq 19$ pC.

We first consider CE of a sphere ($\alpha_0 = 1$) with initial radius $R_0 \simeq 80$ nm. In this simulation, the mesh size in all three directions is as small as $\Delta x = \Delta y = \Delta z = R_0/20$, and 200 macroparticles per cell are used. Figures 8(a) and 8(b) display the temporal evolution of the spheroid radii (normalized to their initial value R_0) and of the maximum kinetic energy normalized to the final energy predicted from the model $\mathcal{E}_S$ (in practical units $\mathcal{E}_S \simeq 12.8$ MeV for present parameters), respectively. Note that these quantities have been extracted along all three spatial directions (x, y, and z), confirming that the CE dynamics remains spherical within a $\simeq$2% error. Furthermore, an excellent agreement is found between our theoretical model and simulations concerning the temporal evolution of both the maximum energy and sphere radius. Figure 8(c) shows the carbon energy distribution at time $t \simeq 10.6\omega_{p0}^{-1}$ (for current parameters $\omega_{p0}^{-1} \simeq 4.6$ fs) and their comparison to theoretical prediction from Eq. (27). Here again, a very good agreement is found between our theoretical model and PIC simulations. It is interesting to see that, also in these simulations, a peak is present at maximum energy. It also originates from a smoothly decreasing ion density at the sphere edge leading to the formation of a shock. In contrast to MD simulations, however, the decreasing density region is not here the result of the discrete particle distribution, but of the projection of the particle density on the mesh. Note also that, at the end of the simulation (at $t \sim 10.6\omega_{p0}^{-1}$), the maximum ion energy reaches $\simeq$85% of its theoretical maximum value (for $\omega_{p0} t \to \infty$), which is in good agreement with the dynamics illustrated in Figs. 3(c) and 3(d).

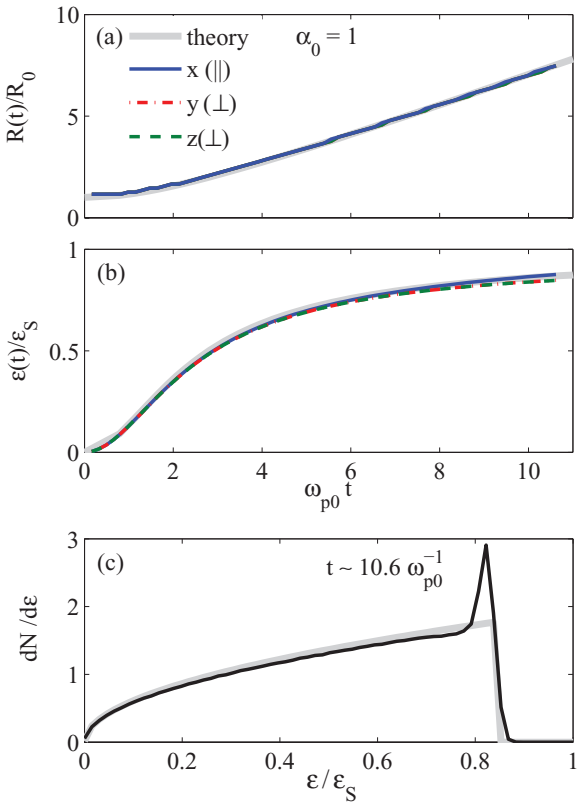

FIG. 8. (Color online) Results from PIC simulations for $\alpha_0 = 1$. (a) Temporal evolution of the sphere radii. (b) Temporal evolution of the maximum kinetic energies. (c) Ion energy spectrum at $t \simeq 10.6\omega_{p0}^{-1}$. Quantities in panels (a) and (b) are presented for all three spatial directions: along the x direction (solid blue), y direction (dot-dashed red), and z direction (dashed green). The thick gray lines show theoretical predictions from our model.

Let us now consider the case of a prolate (cigar-shaped, $\alpha_0 \ll 1$) spheroid with longitudinal radius $w_{\parallel,0} = 4.6R_0$ and transverse radii $w_{\perp,0} = 0.46R_0$ (corresponding to an initial aspect ratio $\alpha_0 = 0.1$). In this simulation, the mesh size is $\Delta x = \Delta y = \Delta z = R_0/10$ and 500 particles per cell have been used. Figures 9(a), 9(b), and 9(c) display the temporal evolution of the normalized spheroid radii and maximum kinetic energies along all three space dimensions, respectively. Figure 9(d) shows the energy distributions at the end of the simulation together with their comparison to theoretical predictions from Eqs. (35), (36), and (37). A fair agreement is found between PIC simulations and analytical predictions.

Finally, the case of an oblate (disk-shaped, $\alpha_0 \gg 1$) spheroid with $\alpha_0 = 10$ ($w_{\parallel,0} = R_0/5$ and $w_{\perp,0} = 2R_0$) is presented in Fig. 10. The mesh sizes in this simulation were set to $\Delta x = R_0/20$ and $\Delta y = \Delta z = R_0/10$ and each cell initially contained 300 particles. The temporal evolution of the normalized radii and normalized maximum kinetic energy along the three spatial directions are displayed in Figs. 10(a), 10(b), and 10(c), respectively. Figure 10(d) shows the energy distributions and their comparison to theoretical predictions from Eqs. (35), (36), and (38). A fair agreement between the PIC simulations and the analytical results is also obtained in this case.

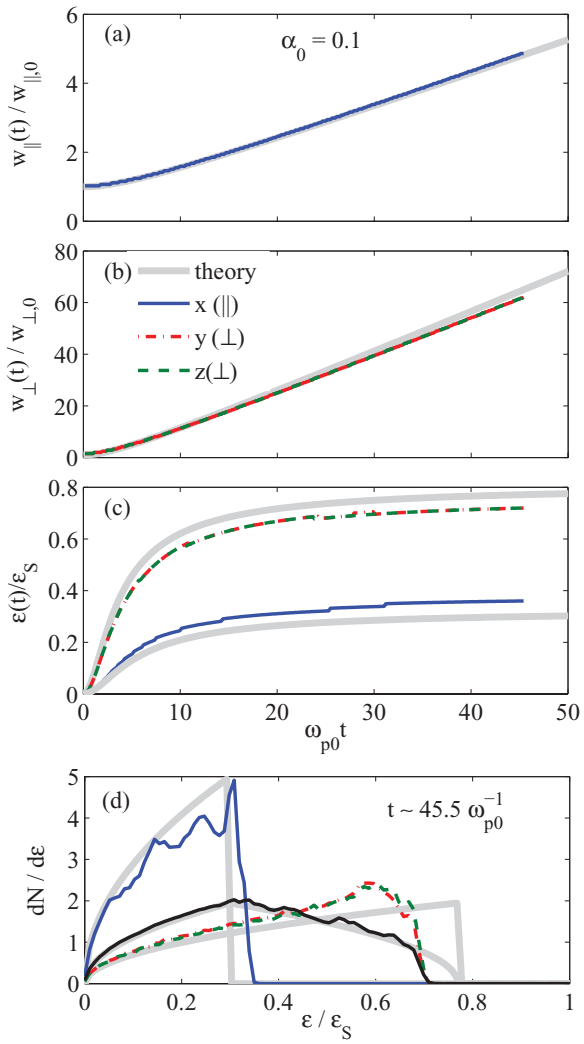

FIG. 9. (Color online) Results from PIC simulations for $\alpha_0 = 0.1$. Temporal evolution of the spheroid radii: (a) in the longitudinal direction and (b) in the transverse direction. (c) Temporal evolution of the maximum energies. (d) Corresponding spectra at $t \simeq 45.5\omega_{p0}^{-1}$; the total spectrum is also shown as a black solid line. Color codes are chosen as in Fig. 7. The thick gray lines show theoretical predictions from our model.

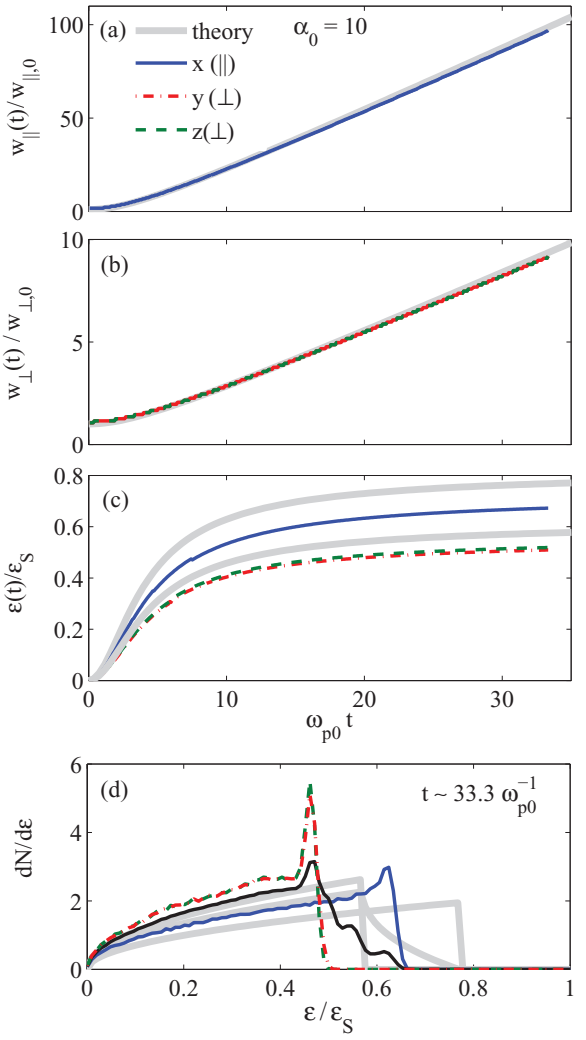

FIG. 10. (Color online) Results from PIC simulations for $\alpha_0 = 10$. Temporal evolution of the spheroid radii: (a) in the longitudinal direction and (b) in the transverse direction. (c) Temporal evolution of the maximum energies. (d) Corresponding spectra at $t \simeq 33.3\omega_{p0}^{-1}$, the total spectrum is also shown as a black solid line. Color codes are chosen as in Fig. 7. The thick gray lines show theoretical predictions from our model.

These simulations demonstrate that our simple model correctly describes the CE dynamics of an initially uniformly charged spheroid. We attribute discrepancies between PIC simulation and our model predictions to the limited resolution of the numerical mesh. Due to technical constraints of our computing facilities, we are currently not able to run simulations with a higher resolution.

V. CONCLUSION

We have developed a simple, semianalytical model for CE of a uniformly charged spheroid. In the limit of nonrelativistic particle velocities, this model gives access to the maximum energy a particle can reach at a given time, the time-dependent particle energy distributions, and the characteristic time of CE. All these quantities can be defined as a function of the spheroid aspect ratio, charge density, and total charge. Our theoretical predictions are found to be in remarkably good agreement with particle (both MD and PIC) simulations.

Because 3D kinetic simulations come at a high computational cost, our results are particularly useful when considering acceleration of ions in the pure CE regime, originating from (spherical or nonspherical) clusters or from thin solid targets. Indeed, our results should be directly applicable in the so-called CVI regime. This regime where electrons are expelled from the cluster on a time much shorter than the characteristic time of ion motion can be accessed by using either ultra-intense lasers or x-ray pulses.

Moreover, with the recent progress in nanotechnology, CE of nanostructured targets can be considered. Our results may thus give us simple design guidelines how to optimize target properties; for example, for inertial fusion applications [38] or to maximize ion collision events for neutron production [39].

Last but not least, our results can also be helpful to model laser–solid-target interaction for ion acceleration, which is characterized by the emission of short, compact, and highly charged ion bunches. Propagation of these bunches (e.g., through a vacuum) is strongly affected by space charge effects [10,11]. By approximating the accelerated ion bunches as uniformly charged spheroids, the results presented here may allow us to derive the conditions required for limited energy and angular dispersions.

ACKNOWLEDGMENTS

Numerical simulations were performed using HPC resources at Rechenzentrum Garching and from GENCI at CCRT and CINES (Grant 2010-x2010056304).

[1] K. Nishihara, H. Amitani, M. Murakami, S. V. Bulanov, T. Zh. Esirkepov, Nucl. Inst. Methods Phys. Res., Sect. A **464**, 98 (2001).
[2] S. Sakabe, S. Shimizu, M. Hashida, F. Sato, T. Tsuyukushi, K. Nishihara, S. Okihara, T. Kagawa, Y. Izawa, K. Imasaki, and T. Iida, Phys. Rev. A **69**, 23203 (2004).
[3] I. Last and J. Jortner, J. Chem. Phys. **121**, 3030 (2004).
[4] Md. Ranaul Islam, U. Saalmann, and J. M. Rost, Phys. Rev. A **73**, 041201 (2006).
[5] A. E. Kaplan, B. Y. Dubetsky, and P. L. Shkolnikov, Phys. Rev. Lett. **91**, 143401 (2003).
[6] V. F. Kovalev and V. Yu. Bychenkov, JETP **101**, 212 (2005).
[7] T. Zh. Esirkepov, S. V. Bulanov, K. Nishihara, T. Tajima, F. Pegoraro, V. S. Khoroshkov, K. Mima, H. Daido, Y. Kato, Y. Kitagawa, K. Nagai, and S. Sakabe, Phys. Rev. Lett. **89**, 175003 (2002).
[8] E. Fourkal, I. Velchev, and C. M. Ma, Phys. Rev. E **71**, 036412 (2005).
[9] S. S. Bulanov, A. Brantov, V. Yu. Bychenkov, V. Chvykov, G. Kalinchenko, T. Matsuoka, P. Rousseau, S. Reed, V. Yanovsky, D. W. Litzenberg, K. Krushelnick, and A. Maksimchuk, Phys. Rev. E **78**, 026412 (2008).
[10] M. Grech, S. Skupin, R. Nuter, L. Gremillet, and E. Lefebvre, New J. Phys. **11**, 093035 (2009); Nucl. Instrum. Methods Phys. Res., Sect. A **620**, 63 (2010).
[11] V. T. Tikhonchuk, Nucl. Instrum. Methods Phys. Res., Sect. A **620**, 1 (2010).
[12] M. Hashida, H. Mishima, S. Tokita, and S. Sakabe, Opt. Express **17**, 13116 (2009).
[13] U. Saalmann, Ch. Siedschlag, and J. M. Rost, J. Phys. B **39**, R39 (2006).
[14] R. C. Davidson, *Physics of Nonneutral Plasmas* (Imperial College Press, London, 2001).
[15] Yu. K. Batygin, Phys. Plasmas **8**, 3103 (2001).
[16] G. Fubiani, J. Qiang, E. Esarey, W. P. Leemans, and G. Dugan, Phys. Rev. ST Accel. Beams **9**, 064402 (2006).
[17] A. Rigo, M. Casas, F. Garcias, E. Moya de Guerra, and P. Sarriguren, Phys. Rev. B **57**, 11943 (1998).
[18] A. Dellafiore, F. Matera, and F. A. Brieva, Phys. Rev. B **61**, 2316 (2000).
[19] K. L. Kelly, E. Coronado, L. L. Zhao, and G. C. Schatz, J. Phys. Chem. B **107**, 668 (2003).
[20] T. C. Killian, T. Pattard, T. Pohl, and J.-M. Rost, Phys. Rep. **449**, 77 (2007).
[21] E. Skopalová, Y. C. El-Taha, A. Zaïr, M. Hohenberger, E. Springate, J. W. G. Tisch, R. A. Smith, and J. P. Marangos, Phys. Rev. Lett. **104**, 203401 (2010) and references therein.
[22] A. Mikaberidze, U. Saalmann, and J. M. Rost, Phys. Rev. Lett. **102**, 128102 (2009).
[23] L. D. Landau and E. M. Lifshitz, *The Classical Theory of Fields, Course of Theoretical Physics*, 4th ed. (Butterworth-Heinemann, Oxford, 2004), Vol. 2, p. 318.
[24] Y. Kiwamoto, H. Aoki, and Y. Soga, Phys. Plasmas **11**, 4868 (2004).
[25] C. C. Lin, L. Mestel, and F. H. Shu, Astrophys. J. **142**, 1431 (1965).
[26] S. Chandrasekhar, *Ellipsoidal Figures of Equilibrium* (Dover Publications, Inc., New York, 1987).
[27] Note that the aspect ratio α_v is a function of time.
[28] D. Frenkel and B. Smit, *Understanding Molecular Simulation* (Academic Press, San Diego, 2002).
[29] W. C. Swope, H. C. Andersen, P. H. Berens, and K. R. Wilson, J. Phys. Chem. **76**, 637 (1982).
[30] M. P. Allen and D. J. Tildesley, *Computer Simulation of Liquids* (Clarendon Press, Oxford, 1991).
[31] F. Peano, R. A. Fonseca, and L. O. Silva, Phys. Rev. Lett. **94**, 033401 (2005).
[32] A. Lévy, R. Nuter, T. Ceccotti, P. Combis, M. Drouin, L. Gremillet, P. Monot, H. Popescu, F. Réau, E. Lefebvre, and P. Martin, New J. Phys. **11**, 093036 (2009).
[33] E. Lefebvre, N. Cochet, S. Fritzler, V. Malka, M.-M. Aléonard, J.-F. Chemin, S. Darbon, L. Disdier, J. Faure, A. Fedotoff, O. Landoas, G. Malka, V. Méot, P. Morel, M. Rabec Le Gloahec, A. Rouyer, Ch. Rubbelynck, V. Tikhonchuk, R. Wrobel, P. Audebert, and C. Rousseaux, Nucl. Fusion **43**, 629 (2003).
[34] C. K. Birdsall and A. B. Langdon, *Plasma Physics via Computer Simulation* (McGraw-Hill, New York, 1985).
[35] A. Taflove and S. C. Hagness, *Computational Electrodynamics: The Finite-Difference Time-Domain Method*, 3rd ed. (Artech House, Norwood, 2005).
[36] J. P. Boris, *Relativistic Plasma Simulations—Optimization of a Hybrid Code*, Proceedings of the 4th Conference on Numerical Simulations of Plasmas, Naval Res. Lab. (Washington DC, 1970), Vol. 3.
[37] T. Zh. Esirkepov, Comput. Phys. Commun. **135**, 144 (2001).
[38] T. Desai, J. T. Mendonca, D. Batani, and A. Bernadinello, *Cluster Induced Ignition—A New Approach to Inertial Fusion Energy*, 18th Fusion Energy Conference, 2000, Sorrento, Italy; proceedings available at [www.iaea.org/programmes/ripc/physics/fec2000/html/node273.html].
[39] T. Ditmire, J. Zweiback, V. P. Yanovsky, T. E. Cowan, G. Hays, and K. B. Wharton, Nature (London) **398**, 489 (1999).